Do We Really Need an Accurate Calibration Pattern to Achieve a Reliable Camera Calibration?

* Jean-Marc Lavest, † Marc Viala, * M.Dhome

* LASMEA
LAboratoire des Sciences et Matériaux pour l'Electronique, et d'Automatique
UMR 6602 du CNRS, Université Blaise-Pascal de Clermont-Ferrand
63177 Aubière cedex. France
lavest@lasmea.univ-bpclermont.fr
† CEA-LETI, Département d'Electronique et d'Instrumentation Nucléaire
Service Logiciels et Architecture
CEA/SACLAY, 91191 Gif-sur-Yvette cedex

Abstract. This article raises the problem of errors caused by the metrology of a calibration pattern to the accurate estimation of the intrinsic and extrinsic calibration parameters modeling the video system. In order to take into account these errors a new approach is proposed that enables us to compute in the same time the traditional calibration parameters and the 3D geometry of the calibration pattern using a multi-images calibration algorithm. Experimental results shows that the proposed algorithm leads to reliable calibration results and proves that calibration errors no longer depend on the accuracy of calibration point measurement, but on the accuracy of calibration point detection in the image plane.

Keys Words
Camera calibration, Calibration pattern, Photogrammetry, Metrology.

1 Introduction

Video cameras are becoming more and more widely used in Computer Vision for 3D measurements. To obtain accurate results, calibration is often necessary in order to determine the intrinsic parameters modeling the video camera system.

Well known calibration technics [Bro71], [Tsa86], [FT87] usually require a 3D known object, called the *calibration target.* This object has to be well defined and accurately measured to insure that the calibration parameters are stable. Nowadays, the wide range of application tasks in robotics has encouraged the use of long focal lengths (i.e. zooming applications [LL96]) as well as very short ones (3.5mm fish-Eye) to obtain a large inspection field. By doing so, it is almost impossible to use the same calibration pattern in the experimental set-up for both zoom and fish-eye applications. Specific patterns have to be setout for a given range of focal lengths.

In order to achieve accurate measurements and calibration results, particular care has to be taken in the way that a 3D calibration pattern is constructed and

also the way the calibration points are measured. This is expensive and time consuming.

In this article we shall examine the influence of errors induced by the metrology of calibration points on the accuracy of the intrinsic calibration parameters. First, we briefly outline the photogrammetric calibration approach used in the article and the way the correlation matrix associated to each camera parameter is estimated. Then, in the second part, the accuracy of the intrinsic camera parameters is analyzed with respect to measurement errors introduced in the 3D calibration points, and also with respect to the 2D errors introduced by the target detection in the camera image plane.

As a result of the conclusions deduced from the previous analysis, a new calibration approach is proposed so that the traditional calibration parameters and the 3D geometry of the calibration pattern can be estimated. Experimental results using first synthetic, then real data, show that the proposed approach enables us to take into account large errors in 3D calibration point measurements.

2 Mathematical Tools for Simultaneous Calibration Using a Least Squares Technique

In our study we use a simplified camera model, i.e., the *pin-hole* model, as depicted in Figure 1. Through this section, the following notations are used:

- W–XYZ is a right-handed 3–D coordinate system as the world reference coordinate system.
- o–uv is the 2–D image pixel system with the origin at the top-left corner of the image.
- o–xy is a 2–D image coordinate system with x and y parallel to those of o–uv and with origin at the principal point o.
- c–xyz is the 3–D camera coordinate system with origin at the optical center c and z-axis coincides with the optical axis and x, y parallel to those of o-xy.

The intrinsic parameters we need to calibrate are: the principal point (u_0, u_0), the focal length f, the pixel sizes of the CCD array or their aspect ratio and the distortion parameters of the optical system.

The extrinsic parameters are the rotation matrix $\boldsymbol{R}$ as well as the translation vector $\boldsymbol{T}$ between W–XYZ and c–xyz.

The method presented in this section is strictly a least squares technique in the sense that we minimize the errors of the measurements. Notations and reference systems are those used in Photogrammetry.

2.1 The Mathematical Model

We assume a perspective projection between a 2–D image and a 3–D object (under the pin-hole camera model). The relationship between a 3–D point and its 2–D image is described by the following equations:

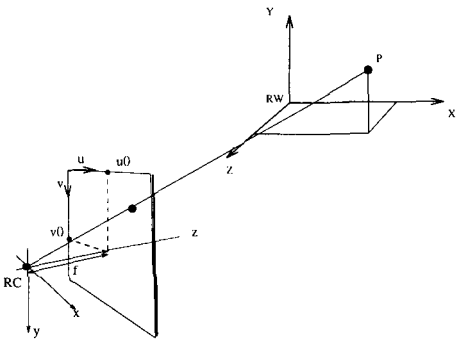

Fig. 1. *The pin-hole camera model, image geometry and coordinate systems.*

$$\begin{pmatrix} x_i \\ y_i \\ z_i \end{pmatrix} = \lambda_i \left[\boldsymbol{R} \begin{pmatrix} X_i \\ Y_i \\ Z_i \end{pmatrix} + \boldsymbol{T} \right] \tag{1}$$

where in (1), (x_i, y_i, z_i) is the image point in the camera system as defined in Figure 1 and $\bar{z}_i \equiv f$, i.e., the focal length of the camera, (u_0, v_0) the coordinates of the principal point, λ_i is a scale factor which maps a point in the camera coordinate system to the image plane, (X_i, Y_i, Z_i) is the object point in the world-coordinate system W–XYZ, (T_x, T_y, T_z) is the translation vector, and $\boldsymbol{R}$ is the rotation matrix, which is constructed by three *independent* rotation angles: α rotating around X-axis, β around Y-axis, and γ around Z-axis:
If we eliminate λ_i in (1) and omit the subscript i, we have the following so-called *collinearity equations* in photogrammetry:

$$\left.\begin{aligned} x &= f\frac{r_{11}X + r_{12}Y + r_{13}Z + T_x}{r_{31}X + r_{32}Y + r_{33}Z + T_z} \\ y &= f\frac{r_{21}X + r_{22}Y + r_{23}Z + T_y}{r_{31}X + r_{32}Y + r_{33}Z + T_z} \end{aligned}\right\} \tag{2}$$

If we transform (x, y) into the pixel coordinate system (u, v), that is

$$\left.\begin{aligned} x &= (u + v_x - u_0)dx - do_x \\ y &= (v + v_y - v_0)dy - do_y \end{aligned}\right\} \tag{3}$$

Here v_x, v_y are errors of the measurements x and y, i.e., corrections to the measurements so that they fit the function values. do_x, do_y are the lens distortion components, which consist of two parts: *radial* and *tangential* distortions, i.e., $do_x = do_{xr} + do_{xt}$ and $do_y = do_{yr} + do_{yt}$. We use two models which are often used in photogrammetry [Ame84]:

$$\left.\begin{aligned} do_{xr} &= (u - u_0)dx(a_1 r^2 + a_2 r^4 + a_3 r^6) \\ do_{yr} &= (v - v_0)dy(a_1 r^2 + a_2 r^4 + a_3 r^6) \end{aligned}\right\} \tag{4}$$

$$\left.\begin{aligned} do_{xt} &= p_1[r^2 + 2(u - u_0)^2 dx^2] + 2p_2(u - u_0)dx(v - v_0)dy \\ do_{yt} &= p_2[r^2 + 2(v - v_0)^2 dy^2] + 2p_1(u - u_0)dx(v - v_0)dy \end{aligned}\right\} \tag{5}$$

where in (3), (4), and (5), u, v are the image coordinates in the pixel system, u_0, v_0 define the principal point in the pixel system, a_1, a_2, a_3 are the radial lens distortion parameters, p_1, p_2 are the tangential distortion parameters, and d_x, d_y are the scale factors of the pixel system in x and y directions respectively, and $r = \sqrt{(u-u_0)^2 + (v-v_0)^2}$, is the radial distance from the principal point.

Substituting (3), (4) and (5) into (2), we have the following:

$$\left.\begin{aligned} u + v_x &= u_0 + (do_{xr} + do_{xt})/dx + (\tfrac{f}{dx})\tfrac{r_{11}X + r_{12}Y + r_{13}Z + T_x}{r_{31}X + r_{32}Y + r_{33}Z + T_z} = P(\boldsymbol{\Phi}) \\ v + v_y &= v_0 + (do_{yr} + do_{yt})/dy + (\tfrac{f}{dy})\tfrac{r_{21}X + r_{22}Y + r_{23}Z + T_y}{r_{31}X + r_{32}Y + r_{33}Z + T_z} = Q(\boldsymbol{\Phi}) \end{aligned}\right\} \quad (6)$$

that can also be rewritten,

$$\left.\begin{aligned} v_x &= P(\boldsymbol{\Phi}) - u \\ v_y &= Q(\boldsymbol{\Phi}) - v \end{aligned}\right\} \boldsymbol{F}(\boldsymbol{\Phi}) \quad (7)$$

As the perspective projection is always defined up to a scale factor, we usually set dx parameter to 1. If we define $f_x = \frac{f}{d_x}$ and $f_y = \frac{f}{d_y}$, the calibration parameters to be estimated have the following expression:

$$\boldsymbol{\Phi} = [u_0, v_0, a_1, a_2, a_3, p_1, p_2, f_x, f_y, T_x, T_y, T_z, \alpha, \beta, \gamma]^T$$

2.2 Solving the Problem

The problem is to estimate the vector $\boldsymbol{\Phi}$ by minimizing $\sum_{i=1}^{n}(v_{x_i}^2 + v_{y_i}^2)$. In (6) $P(\boldsymbol{\Phi})$ and $Q(\boldsymbol{\Phi})$ are non-linear functions of $\boldsymbol{\Phi}$, the minimization is a non-linear optimization problem. One way of solving the problem is to linearize (6) with some initial value $\boldsymbol{\Phi}_0$ and solve for $\boldsymbol{\Delta\Phi}$. Then by adding $\boldsymbol{\Delta\Phi}$ to $\boldsymbol{\Phi}_0$ as the new initial value and repeating the process until a certain convergency is satisfied.

Given n 3D points and their corresponding 2D image points, we can write the $2 \times n$ linearized measurement or error equations in matrix form:

$$\boldsymbol{V} = L + \boldsymbol{A}\,\boldsymbol{\Delta\Phi} \quad (8)$$

$$with \qquad L = \boldsymbol{V}(\boldsymbol{\Phi_0}) \qquad and \qquad \boldsymbol{A} = \boldsymbol{F}'_{\boldsymbol{\Phi}_0} = \frac{\delta F}{\delta \Phi_{|\boldsymbol{\Phi}=\boldsymbol{\Phi}_0}}$$

Let the weight matrix of the measurements be $\boldsymbol{W}$, the least squares solution to (8) is a minimization problem of

$$\min_{\boldsymbol{\Delta\Phi} \in \Re^{15}} \left(\boldsymbol{V}^T \boldsymbol{W} \boldsymbol{V}\right) \quad (9)$$

The solution to (9) can be obtained as:

$$\boldsymbol{\Delta\Phi} = (\boldsymbol{A}^T \boldsymbol{W} \boldsymbol{A})^{-1} (\boldsymbol{A}^T \boldsymbol{W} \boldsymbol{L}) \quad (10)$$

2.3 Multi-image Calibration

One major source of calibration errors is the results of measurement errors. These errors can be located on the 3d coordinates of the calibration points but also in the image plane when the target point coordinates are estimated.

One way to improve this is to combine more than one image taken by the same camera but from different (rotated and/or translated) positions. In such a case, the intrinsic parameters remain the same for all images and the calibration task means computing a parameter vector of

$$\boldsymbol{\Phi}_{9+6m} = \Big[u_0, u_0, a_1, a_2, a_3, p_1, p_2, f_x, f_y, T_x^1, T_y^1, T_z^1, \alpha^1, \beta^1, \gamma^1, \cdots, T_x^m, T_y^m, T_z^m, \alpha^m, \beta^m, \gamma^m\Big]^T$$

If m is the number of images and n is the number of points on each image, the total number of equations will be $(2mn)$ and the total number of parameter is $(9 + 6m)$. The redundancy number r is $r = 2mn - 9 - 6m$, which is much larger than the one in the single-image calibration case. As we will show in the next subsection, the larger the redundancy the higher the reliability.

An important advantage of the multiple images approach is to provide a better estimate of distorsion paramaters when a short focal length has to be calibrated. Actually, in most application cases, the calibration target only covers a short part of the image. Using a multiple images approach, you can move the camera to obtain measurement information in all the CCD matrix surface and insure the radial parameters are more reliable.

3 Accuracy Assessment

3.1 Theoretical point of view

From the least squares estimation of (8) and (9), we can compute the estimates of the residual vector $\boldsymbol{V}$ as

$$\hat{\boldsymbol{V}} = [\boldsymbol{I} + \boldsymbol{A}(\boldsymbol{A}^T\boldsymbol{W}\boldsymbol{A})^{-1}\boldsymbol{A}^T\boldsymbol{W}]\boldsymbol{L} \tag{11}$$

and the estimate of the so called *standard error of unit weight*, which is the posteriori estimation of the noises σ_0 of the image coordinates if the model is correct and there are no system errors:

$$\hat{\sigma}_0^2 = \frac{\boldsymbol{V}^T\boldsymbol{W}\boldsymbol{V}}{N - r} \tag{12}$$

and the estimate of the *covariance* matrix of the parameters $\boldsymbol{\Phi}$:

$$\boldsymbol{C}_{\boldsymbol{\Phi}} = (\boldsymbol{A}^T\boldsymbol{W}\boldsymbol{A})^{-1} \tag{13}$$

And for each individual parameter ϕ_i, we can then compute the estimate of its precision, or the standard deviation:

$$\hat{\sigma}_{\phi_i}^2 = \hat{\sigma}_0^2 c_{ii} \tag{14}$$

3.2 Experimental factors

There are many factors which affect the accuracy of the computed parameters, and thus the reconstructed 3D data using these parameters. In the previous paragraph we have shown some error sources. Let us summarize the major factors:

- The number and accuracy of the measurements. How well we can measure 2D points in the image, and the accuracy of the 3D object points are the main factor which effect the accuracy of the calibration. Usually, we assume the 3D points are free of error, which is not quite true. Assuming both errors are random errors (with a certain distribution), this type of error will result in a random residual error in the image after the least squares adjustment.
- Geometrical configuration of the set up, i.e., the relation between the camera and the calibration object. This factor determines the internal strength of the least squares solution, i.e., the design matrix $\boldsymbol{A}$ of the system. Improper geometrical configuration will result in poor accuracy and reliability [LL96].
- The mathematical models used for the calibration. We model the camera lens as a *pin-hole* model, which is just an approximation, and so the lens distortion is modelled as radial and tangential distortion. The lens system is a very complicated optical and mechanical construction, and there is no exact model for it. The imperfect model will result in a systematic error in the image after the calibration.
- Jitter effects can also be underlined. They are directly influenced by with the electronic stability of the frame grabber, and [Bey92] shows that their influence can induce systematic errors in the video images - up to 0.5 pixel.

3.3 Influence of the calibration pattern

The influence of the calibration pattern on the parameters estimated during the calibration process can be analysed in different ways.

In [LL96] the authors show that the geometrical configuration of the calibration pattern (several grids, cubes ...) is highly connected to the correlation matrix form of the computed parameters.

In this section we want to analyse the influence of random errors introduced in the coordinates of the calibration points, on the accuracy of the computed parameters.

Experimental setup

Let us define a set of 11 synthetic images, that represents a calibration pattern of 11 points observed with a video camera equipped with a 10mm lens. The image set is computed in order to allow the calibration pattern to be observed from highly different view points.

Table 1 describes the calibration results obtained for different ranges of noise (in millimeters) introduced in the coordinates (x,y,z) of the calibration points. The total dimensions of the calibration object are approximately ($0.6 \times 0.6 \times 0.4m^3$). The target is observed at a mean distance of $1.5m$.

Table 1. Calibration results in relation to a gaussian noise added to the coordinates x, y, z of the calibration points

noise (x,y,z) 0.0 mm^3	
σ_0 = *0.0 (pix)*	
fx(pix) = 1670.0	σfx= 1.0e-9
fy(pix) = 1671.0	σfy= 1.0e-9
u0(pix) = 391.0	$\sigma u0$= 1.0e-9
v0(pix) = 278.0	$\sigma v0$= 1.0e-9

noise (x,y,z) 0.01mm^3		*noise (x,y,z) 0.1mm^3*	
σ_0 = *0.006 (pix)*		σ_0 = *0.05 (pix)*	
fx= 1668.92	σfx= 0.21	*fx*= 1659.68	σfx= 2.12
fy= 1669.98	σfy= 0.21	*fy*= 1661.24	σfy= 2.15
u0= 391.27	$\sigma u0$= 0.15	*u0*= 393.66	$\sigma u0$= 1.55
v0= 277.89	$\sigma v0$= 0.17	*v0*= 277.10	$\sigma v0$= 1.72

noise (x,y,z) 0.5mm^3		*noise (x,y,z) 2.0mm^3*	
σ_0 = *0.28 (pix)*		σ_0 = *1.16 (pix)*	
fx= 1626.55	σfx= 10.26	*fx*= 1610.26	σfx= 44.04
fy= 1630.40	σfy= 10.36	*fy*= 1623.36	σfy= 44.59
u0= 402.47	$\sigma u0$= 7.42	*u0*= 422.83	$\sigma u0$= 30.01
v0= 276.10	$\sigma v0$= 8.13	*v0*= 296.10	$\sigma v0$= 32.00

$\sigma 0$ represents the standard deviation of unit weight estimated from expression (12). The standard deviation associated to each parameter of the calibration vector is estimated from expression (14). The first experiment is performed without adding any noise. It gives the synthetical calibration results according to the images set.

Through these tables, we can notice the major infuence of the metrological quality of the calibration target on the accuracy of the calibration results.

It can be underlined:

- on the one hand that the intrinsic parameters are soon affected by a random noise added on target points,
- moreover that an error greater than ($2mm^3$) leads to the non-convergence of the optimization process. This critical value is conditionned by the experimental setup. For example the calibration of a fish-eye lens will lead to the non covergence of the algorithm for a smaller value of measurement errors.

Noise added to each calibration point coordinates, was generated during this experimental setup, under a uniform law. The influence of the calibration pattern metrology could also be analysed with systhematic errors introduced, for example by the non orthogonality between the different faces of a calibration cube.

3.4 Influence of calibration point detection

Table 2. Calibration results in relation to a gaussian noise added to calibration point detection in the image plane

noise (u,v) 0.0 pix²	
σ_0 = *0.0 (pix)*	
fx(pix) = 1670.0	σfx= 1.0e-9
fy(pix) = 1671.0	σfy= 1.0e-9
u0(pix) = 391.0	$\sigma u0$= 1.0e-9
v0(pix) = 278.0	$\sigma v0$= 1.0e-9

noise (u,v) 0.02 pix²		*noise (u,v) 0.05 pix²*	
σ_0 = *0.02 (pix)*		σ_0 = *0.05 (pix)*	
fx= 1670.16	σfx= 0.77	*fx*= 1670.58	σfx= 1.94
fy= 1671.24	σfy= 0.78	*fy*= 1671.79	σfy= 1.96
u0= 391.66	$\sigma u0$= 0.56	*u0*= 392.63	$\sigma u0$= 1.41
v0= 278.76	$\sigma v0$= 0.63	*v0*= 279.93	$\sigma v0$= 1.58

noise (u,v) 0.5 pix²		*noise (u,v) 1.0 pix²*	
σ_0 = *0.51 (pix)*		σ_0 = *1.06 (pix)*	
fx= 1704.82	σfx= 20.63	*fx*= 1837.14	σfx= 51.85
fy= 1708.11	σfy= 20.77	*fy*= 1842.94	σfy= 52.00
u0= 402.92	$\sigma u0$= 14.70	*u0*= 400.93	$\sigma u0$= 33.58
v0= 303.34	$\sigma v0$= 16.53	*v0*= 346.98	$\sigma v0$= 40.94

Experimental setup

The experimental setup remains similar to the previous one. In this section the 3D coordinate of the calibration points are supposed to be noise free.

Table 2 describes experimental calibration results obtained for different ranges of noise (in pixel) added to each coordinate (u, v) of the calibration points projected in the image plane.

The first table, which is noise free, gives the theoretical solution according to the synthetic data. The noise ranges used in this experiment are classified from an accurate subpixel detector ($\sigma 0 = 0.02pix$) to a rough estimate of the calibration point coordinates ($\sigma 0 = 1.0pix$) .

A precise analysis of the table shows that accurate calibration results can only be achieved with a **subpixel detector**. Errors greater than $0.5pix$ in coordinate point estimates lead to significant variation in the calibration parameters.

4 New Calibration Formulation

High quality calibration patterns are often difficult to achieve. They have to be mechanically stable in time (compared with the temperature change), and an accurate measurement of the location of points carried out by a metrology company is expensive. Futhermore, the large range of application fields in robotics means we use short as well as long focal lengths. This implies that the laboratory must have several calibration patterns associated to specified applications.

Is it possible inside a multiple images calibration approach to estimate the calibration point coordinates in space at the same time as the intrinsic and extrinsic calibration parameters ?

Let us rewrite the colinearity equations:

$$\left.\begin{aligned} u + v_x &= u_0 + (do_{xr} + do_{xt})/dx + (\tfrac{f}{dx})\tfrac{r_{11}X+r_{12}Y+r_{13}Z+T_x}{r_{31}X+r_{32}Y+r_{33}Z+T_z} = P(\boldsymbol{\Phi}) \\ v + v_y &= v_0 + (do_{yr} + do_{yt})/dy + (\tfrac{f}{dy})\tfrac{r_{21}X+r_{22}Y+r_{23}Z+T_y}{r_{31}X+r_{32}Y+r_{33}Z+T_z} = Q(\boldsymbol{\Phi}) \end{aligned}\right\} \quad (15)$$

The new calibration vector to be determined, if the 3D coordinates of calibration points have to be estimated with the traditional calibration parameters, takes the following form:

$$\boldsymbol{\Phi}_{9+6m+3*n} = \Big[u_0, v_0, a_1, a_2, a_3, p_1, p_2, f_x, f_y, X^1, Y^1, Z^1, \cdots, X^n, Y^n, Z^n, T_x^1, T_y^1, T_z^1, \alpha^1, \beta^1, \gamma^1, \cdots, T_y^m, T_z^m, \alpha^m, \beta^m, \gamma^m\Big]^T$$

where n represents the total number of target points and m the total number of images taken during the calibration setup.

4.1 Redundancy

Total number of unknown parameters :

9 (intrinsic parameters) + 3*n (calibration point coordinates) + 6*m (extrinsic parameters).

Number of equations : 2*m*n.

The redundancy of the system to be solved, $r = 2*m*n - (9 + 3*n + 6*m)$, can be obtained easily. According to the the synthetic experiments previously used, in which the calibration pattern was achieved with 11 points ($n = 11$), a minimal set of 3 images is sufficient to over-determine the system.

4.2 Initial conditions to insure algorithm convergency

The system to be solved is a non-linear optimisation. It requires an initial value of the calibration vector not too far from the solution in order to insure algorithm convergency.

In the final experimental results, we will show that this initial value is not really difficult to obtain, and that a good convergency can be achieved if the

calibration views of the pattern are taken from different orientation observations. This is equivalent to insuring very constrained triangulation angles in space for the 3D point reconstruction. As underlined in [Bro71], we have noticed that multiple views taken with a 90 degree rotation around the optical axis leads to a better estimate (better convergency and better accuracy) of the calibration parameters.

4.3 Calibration solution determined up to a scale factor

1. Intrinsic parameters
   In the traditional approach to photogrammetric calibration, the intrinsic parameters are always determined up to a scale factor. The usual assignation of the x-size of the CCD matrix to one ($dx = 1$), means the other parameters can be expressed in an arbitrary unit defined in pixels.
2. Extrinsic parameters
   Since the 3D coordinates of the calibration points are simultaneously estimated with the calibration parameters, the extrinsic geometry of the vision system is also determined up to a scale factor. Actually, in these conditions the reconstruction of a bigger calibration pattern observed from a farther distance will provide an identical image.
   This loss of metric dimension does not have great consequences on a single camera calibration. Key information for further application tasks are only contained in the intrinsic parameters. Let us recall that extrinsic parameters gives the 3D location of the calibration pattern, expressed in the camera frame, and in accordance with a given view of the image set. However if a stereo (or more) vision system has to be calibrated it will be necessary to introduce a metric dimension to fix the extrinsic geometry of the camera configuration. Such a task can easily be performed with the accurate knowledge of the euclidian distance between 2 points among n.

5 Experimental results

In this section, an experimental study is performed. It is divided into two parts. first, synthetic data previously used is tested with the new calibration approach. Then, the algorithm is evaluated with real data taken from camera devices equipped with different fixed focal-lens lenses.

5.1 Synthetic data

Without noise on image point detection

In this sub-section the experimental conditions used to create the synthetic data set remain the same as those defined in section 3.2. A random noise (inside a given standard deviation) is added to each coordinate of the 3D calibration points. Point detection in the image plane is first of all supposed to be noise free.

Table 3. Calibration results from synthetic data in relation to a gaussian noise added to the calibration point coordinates

	Starting conditions (fx=3000 fy=3000) (u0=300 v0=300)							
noise	*convergency*				*results*			
xyz mm^3	*nb itera*	*k*	σ_k	*fx (pix)*	*fy (pix)*	*u0 (pix)*	*v0 (pix)*	
0.01	45	0.9838	0.0	1670	1671	391	278	
0.1	45	0.9838	0.0	1670	1671	391	278	
1.0	47	0.9832	0.0	1670	1671	391	278	
10.0	48	0.9767	0.0	1670	1671	391	278	

Table 3 shows that the new calibration formula enables us to take into account errors (up to $10.0mm^3$) introduced into the calibration pattern and converges at any time to the same values of intrinsic parameters. Note, that the starting conditions are far from the true solution and are directely correlated to the number of iterations required by the process to find the solution.

Parameter k indicates the scale factor of the extrinsic geometry obtained at the convergency. It is estimated as followed

$$k = \frac{1}{n-1} \sum_{i=2}^{n} \frac{|P_i - P_{i-1}|}{|\hat{P}_i - \hat{P}_{i-1}|} \tag{16}$$

where P_i is a reconstructed points of the calibration pattern and $\hat{P}_i$ its corresponding point in the true solution.

σ_k gives the standard deviation of this distribution. In table 3 it can be noted that σ_k is systematically equal to zero, because the algorithm has accurately estimated the calibration target geometry, as well as the intrinsic and extrinsic parameters that give the perfect correspondance of colinearity equations (6). Results described in this table have to be compared with experiment Table 1 using the traditional calibration formulation.

Adding noise to image point detection

For this experiment two different noises added on each image coordinate have been considered (respectively 0.01 pix and 0.1 pix). Given an image noise, the 3d coordinates of all the calibration points have been modified using a gaussian distribution with a standard deviation of respectively $0.1mm^3$ and $10.0mm^3$.

For a given range of image noise (0.01 and 0.1 pix), the analysis in table 4 shows that the algorithm computes the same extrinsic geometry of the calibration set-up (up to a scale factor) and converges to the same values of the intrinsic parameters (focal length, principal point).

Table 4. Calibration results from synthetic data in relation to a gaussian noise added to the calibration points coordinates and the image point detection

Initial conditions (fx=3000 fy=3000) (u0=300 v0=300)		*(results in pixel)*	
image noise (u,v) 0.01 pix			
calib. target noise (x,y,z) $0.1mm^3$		*calib. target noise (x,y,z)* $10.0mm^3$	
fx= 1666.64	σ = 0.35	*fx*= 1666.64	σ = 0.35
fy= 1668.03	σ = 0.36	*fy*= 1668.03	σ = 0.36
u0= 391.49	σ = 0.26	*u0*= 391.49	σ = 0.26
v0= 278.73	σ = 0.31	*v0*= 278.73	σ = 0.31
nb itera=47		*nb itera=48*	
$\sigma 0$=*0.01*		$\sigma 0$=*0.01*	
k = 0.97538	σ = 0.000101	*k*= 0.97433	σ = 0.000103
image noise (u,v) 0.1 pix			
calib. target noise (x,y,z) $0.1mm^3$		*calib. target noise (x,y,z)* $10.0mm^3$	
fx= 1651.35	σ = 3.50	*fx*= 1651.35	σ = 3.50
fy= 1652.99	σ = 3.54	*fy*= 1652.99	σ = 3.54
u0= 396.03	σ = 2.60	*u0*= 396.03	σ = 2.60
v0= 285.10	σ = 3.01	*v0*= 285.10	σ = 3.01
nb itera=48		*nb itera=49*	
$\sigma 0$=*0.094*		$\sigma 0$=*0.094*	
k = 0.97538	σ = 0.000910	*k*= 0.97433	σ = 0.000910

Conclusion

The calibration errors compared with the true synthetic solution no longer depend on the accuracy of the calibration point measurement, but on the accuracy of calibration point detection in the image plane. The first part of table 4 indiquates that a subpixel (0.01pix) point detector leads to calibration results very close to the true solution even if the 3d calibration points are estimated roughly. It can be underlined that a good numerical convergency of the algorithm greatly depends on the choice of the target observation points of view.

5.2 Real Data

Test sequence n-1 Table 5 describes the results of a traditional multiple-images calibration algorithm, experimented on a set of 11 images. The target pattern is composed of 30 points. The tridimensional geometry of the calibration points is known with an accuracy of $0.02mm^3$. The total volume of the calibration pattern is equal to $(0.6 \times 0.6 \times 0.4m^3)$. Each calibration point is obtained using

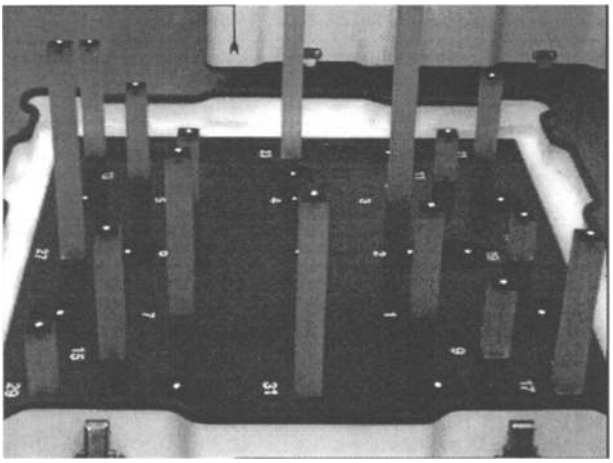

Fig. 2. CEA calibration pattern

a photo-reflector material to insure an accurate detection.

Data was tested in two different laboratories and algorithms were also implemented in C and Fortran with two different numerical optimisation librairies (Numerical Recipies and dMinPack).

The classical calibration approach leads to a residual value of 0.033 and 0.026 pixel respectively along the coordinates (u,v) of the 289 measurement points. According to a recent experiment performed by the European Space Agency (ESA) [Pa97], these results seem quite good.

Table 6 describes results obtained with the new calibration algorithm. Solution of intrinsic parameters are quite similar. The residual value at convergency is slightly smaller. Even if calibration points coordinates are modified (noise up to $10.0mm^3$), the solution at convergency remains the same.

As the true values of the calibration points are known in this section, the factor σk gives us information about the relationship between the reconstructed target and the true one. We can notice that modification of $1.2e-4\%$ has been found by the algorithm to allows a better fitting of the colinearity equations.

Conclusion

To conclude, we can say that while accurate observation of n points from a set of m different points of view is possible, an accurate knowledge of the 3d calibration point coordinates does not seem to be necessary to achieve accurate values of intrinsic calibration parameters.

Test sequence n-2 In this experiment, our aim is to achieve calibration of a fisheye lens (3.8mm) that induces a high radial distorsion in the image plane. The target used for calibration was rapidely setup using two little circular objects composed of 12 photo-reflector points.

Table 5. Calibration results on real data

camera	: Sony XC75CE
lens	: 10mm Angénieux
frame grabber	: Silicon Graphics
algorithm	: Traditional multiple image calibration
calibration target	: CEA-Saclay

Number of images	: 11
Number of measurements	: 289

vx residual: mean and std-dev (pix)	-9.150e-06	3.344e-02
vy residual: mean and std-dev (pix)	1.233e-05	2.634e-02
Std error of unit weight (pix)		3.686107e-02

		σ				σ
fx(pix)	1672.89	2.08e-01		a1	1.538e-01	5.12e-03
fy(pix)	1676.03	2.09e-01		a2	-8.758e-01	1.44e-0
u0(pix)	386.74	4.26e-01		a3	6.121e+00	1.23e+00
v0(pix)	276.86	3.65e-01		p1	6.478e-04	7.12e-05
				p2	7.684e-05	6.41e-05

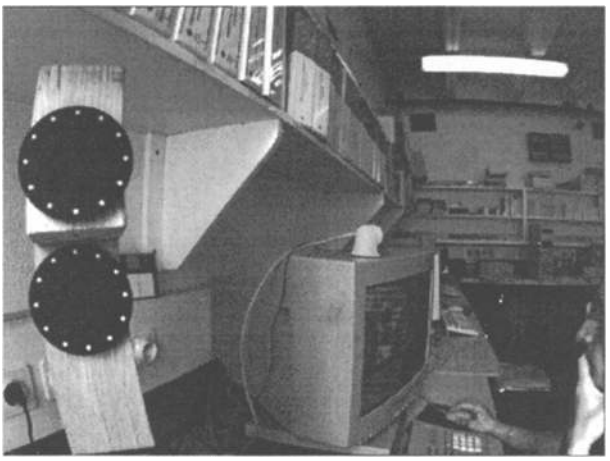

Fig. 3. Fish-eye calibration

The geometry of each elementary target was roughly known ($\simeq 1mm$). The relative location between the two objects was set to zero at the begining of the process convergency. Figure 3 shows one of the eight views used during the

Table 6. Calibration results on real data with added noise on the 3D coordinates of the calibration points

New approach

camera	: Sony XC75CE
lens	: 10mm Angénieux
frame grabber	: Silicon Graphic
algorithm	: New Approach.

Number of images	: 11
Number of measurements	: 271

vx residual: mean and std-dev (pix)	2.934e-07	1.875e-02
vy residual: mean and std-dev (pix)	-5.486e-09	1.337e-02
Std error of unit weight (pix)		1.972624e-02
scale factor ($\bar{k}$ and σk)	0.98733	0.00012

		σ				σ
fx(pix)	1672.85	1.33e-01		a1	1.458e-01	3.20e-03
fy(pix)	1675.96	1.34e-0		a2	-6.749e-01	9.02e-0
u0(pix)	386.48	2.68e-01		a3	4.685e+00	7.69e-01
v0(pix)	277.26	2.34e-01		p1	5.960e-04	4.44e-05
				p2	5.599e-05	4.04e-05

calibration setup and shows the radial distorsion phenomenon. During the images sequence the camera is moved to obtain measurement points throughout all the CCD surface.

We must underline that approximate knowledge of the circular object allows us to compute an initial value of rotation and translation parameters (R_i, T_i) that locates the target in each image. We hope in further works to improve this point using shape from motion approaches as those proposed by Kanade [PK94].

In this experiment (table 7), the new calibration approach enables us to reconstruct the calibration pattern and provides a solution of intrinsic parameters leading to quite small residual values (0.030 et 0.026 pix). The standard deviation for this last experiment is larger than for the previous data set (Tab 6). The difference is mainly due to the less accurate adequation of the distorsion model in this case.

Table 7. Calibration results with real data

New approach

camera	: JAI M50
lens	: 3.8mm Ernitec
frame grabber	: Silicon Graphics
algorithm	:new approach.

Nomber of images	: 8
Nomber of measurements	: 185

vx residual mean and std-dev (pix)	-7.135e-05	3.080e-02
vy residual mean and std-dev (pix)	-6.216-05	2.663e-02
Std error of unit weight (pix)		3.565e-02

		σ				σ
fx(pix)	459.70	2.65e-01		a1	3.746e-01	1.56e-03
fy(pix)	460.44	2.67e-01		a2	1.120e-01	4.58e-03
u0(pix)	365.97	2.26e-01		a3	1.729e-01	4.68e-03
v0(pix)	299.96	2.49e-01		p1	4.635e-04	1.03e-04
				p2	-1.232e-03	1.15e-04

6 Discussion and Conclusion

Calibration point detection

Accuracy of calibration parameters achieved by the algorithm described in this article is greatly dependent on the quality of calibration point detection in the image plane. We have shown with synthetic data that a sub-pixel detector (0.01 or 0.02 accurate) leads to almost perfect calibration parameters.

In practice, we have noticed that the sub-pixel detection of image dots gives more reliable results than cross detection. In [Pa97] the authors arrive at the same conclusions. Experimental results described in the paper use a subpixel spot detector based on an affine transformation associated with a scale factor, that transform the photonic response of a theoretical spot to fit the image content. Experimental accuracy achieved by this way is less than 0.02 pixel.

Introduction of a metric distance

As previously stated the extrinsic geometry between the different points of view of the calibration set-up is determined up to a scale factor. To eliminate this unknown factor, it is sufficient to introduce among the n calibration points the distance between 2 points. Actually, we can imagine that each calibration

pattern is roughtly achieved in connection with the adopted focal-length. An accurate metric distance determined by two photoreflector points in a very stable material (invar) could be added in the set of calibration images. The final cost of the calibration pattern is limited to the accurate measurement of the distance between these two points. Most optical firms can provide this kind of calibration metrics.

Convenient to use

The calibraton algorithm described in this article is really convenient to use, and makes it possible to obtain rapid, perfectly defined calibration targets for short as well as long focal-lengths. The residual values obtained during the experiments are similar to those given by traditional algorithms, and show the reliability of the proposed algorithm. In practice, the convergency is assured without problem if the 3d geometry of the target is approximately known. For critical cases where no 3D information is available, we usually start the process with a flat model located in front of the camera. This case could be improved by starting the algorithm with an initial value given by a shape from motion estimator.

Further works

Instead of using photo-reflector calibration points that are well defined in the images, we should like to experiment the same approach on natural scenes. Using texture information contained about specific points of interest, we are working on accurate matching between these points along the set of calibration images. In this way we hope to perform accurate camera calibration with natural textured objects.

References

[Ame84] American Society for Photogrammetry. *Manual of Photogrammetry*, 4th edition, 1984.

[Bey92] H.A. Beyer. *Geometric and Radiometric Analysis of a CCD-Camera Based Photogrammetric Close-Range System.* PhD thesis, Institut fur Geodasie und Photogrammetrie, Nr 51, ETH, Zurich., May 1992.

[Bro71] D.C. Brown. Close-range camera calibration. *Photogrammetric Engineering*, Vol 8(Nr 37):pp 855–866, 1971.

[FT87] O. Faugeras and G. Toscani. Camera calibration for 3d computer vision. In *Proc. of CVPR*, Tokyo, japan, 1987.

[LL96] M. Li and JM. Lavest. Some aspects of zoom lens calibration. *IEEE PAMI*, Vol 18(Nr 11), 1996.

[Pa97] P. Plancke and al. Calibration of vision system (calvin). *Final Report of European Space Agency*, (WPB5-T1), 1997.

[PK94] C.J. Poelman and T. Kanade. A paraperspective factorisation method for shape and motion recovery. *Third European Conference on Computer Vision,ECCV94,Stockholm*, Vol 2:pp 97–108, May 1994.

[Tsa86] R.Y. Tsai. An efficient ansd accurate calibration technique for 3d machine vision. In *In proc. of CVPR*, pages pp 364–374, Miami, UsA, 1986.